MBNL deficiency in motor neurons disrupts neuromuscular junction maintenance and gait coordination

Charles Frison-Roche, Célia Martin Demier, Steve Cottin, Jeanne Lainé, Ludovic Arandel, Marius Halliez, Mégane Lemaitre, Xavière Lornage, Laure Strochlic, Maurice Swanson, et al.

BRAIN
ORIGINAL ARTICLE

MBNL deficiency in motor neurons disrupts neuromuscular junction maintenance and gait coordination

Charles Frison-Roche,[1] Célia Martin Demier,[1] Steve Cottin,[1] Jeanne Lainé,[1] Ludovic Arandel,[1] Marius Halliez,[1] Mégane Lemaitre,[2] Xavière Lornage,[1] Laure Strochlic,[1] Maurice S. Swanson,[3] Cécile Martinat,[4] Julien Messéant,[1] Denis Furling[1,†] and Frédérique Rau[1,†]

[†]**These authors contributed equally to this work.**

Muscleblind-like proteins (MBNLs) are a family of RNA-binding proteins that play essential roles in the regulation of RNA metabolism. Beyond their canonical role in RNA regulation, MBNL proteins have emerged as key players in the pathogenesis of myotonic dystrophy type 1. In myotonic dystrophy type 1, sequestration of MBNL proteins by expansion of the CUG repeat RNA leads to functional depletion of MBNL, resulting in deregulated alternative splicing and aberrant RNA processing, which underlie the clinical features of the disease.

Although attention on MBNL proteins has focused on their functions in skeletal muscle, new evidence suggests that their importance extends to motor neurons (MNs), pivotal cellular components in the control of motor skills and movement. To address this question, we generated conditional double-knockout (dKO) mice, in which *Mbnl1* and *Mbnl2* were specifically deleted in motor neurons (MN-dKO). Adult MN-dKO mice develop gait coordination deficits associated with structural and ultrastructural defects in the neuromuscular junction, indicating that MBNL activity in MNs is crucial for the maintenance of the neuromuscular junction. In addition, transcriptome analysis performed on the spinal cord of MN-dKO mice identified mis-splicing events in genes associated with synaptic transmission and neuromuscular junction homeostasis.

In summary, our results highlight the complex roles and regulatory mechanisms of MBNL proteins in MNs for muscle function and locomotion. This work provides valuable insights into fundamental aspects of RNA biology and offers promising avenues for therapeutic intervention in myotonic dystrophy type 1 and in a range of diseases associated with RNA dysregulation.

1 Centre de Recherche en Myologie, Sorbonne Université, Inserm, Institut de Myologie, 75013 Paris, France
2 UMS28, Phénotypage du Petit Animal, Sorbonne Université, 75013 Paris, France
3 Department of Molecular Genetics and Microbiology, Center for NeuroGenetics and the Genetics Institute, University of Florida, College of Medicine, Gainesville, FL 32610, USA
4 Inserm, Paris Saclay University, I-STEM, 91100 Corbeil-Essonnes, France

Correspondence to: Frédérique Rau
Centre de Recherche en Myologie—INSERM UMRS 974 Sorbonne Université—Institut de Myologie
G.H. Pitié-Salpétrière, 75013 Paris, France
E-mail: frederique.rau@sorbonne-universite.fr

Received April 26, 2024. Revised August 09, 2024. Accepted October 02, 2024. Advance access publication October 26, 2024

Correspondence may also be addressed to: Denis Furling
E-mail: denis.furling@sorbonne-universite.fr

Keywords: MBNL; RNA binding protein; alternative splicing; neuromuscular junction; motor neurons; myotonic dystrophy type 1

Introduction

Muscleblind-like proteins (MBNLs) are a family of RNA-binding proteins whose primary function lies in their ability to bind specific RNA motifs, particularly the YGCY sequence, through their zinc finger domains.[1] By binding to these RNA motifs, MBNL proteins can influence alternative splicing, mRNA stability, alternative polyadenylation and microRNA processing through interaction with target transcripts.[2–5] MBNL proteins are crucial for normal development and function of various tissues, including skeletal muscle, heart and brain. In mammals, there are three known MBNL genes: *MBNL1*, *MBNL2* and *MBNL3*. Besides their structural resemblance, MBNL proteins differ in their expression pattern. MBNL1 and MBNL2 are ubiquitously expressed, although the highest MBNL1 expression level has been reported in heart and skeletal muscles, where MBNL2 is predominantly present in the CNS.[6] Remarkably, MBNL1 and MBNL2 could have compensatory roles, and the loss of either MBNL1 or MBNL2 results in a significant increase of the other paralogue, associated with partial functional compensation. The importance of this dependence is emphasized further by the fact that double MBNL1- and MBNL2-deficient mice are embryonic lethal.[7,8] MBNL proteins have been described as key players in the pathogenesis of myotonic dystrophy type 1 (DM1). DM1 is an autosomal dominant multisystemic disorder characterized by progressive muscle weakness and wasting, myotonia, cardiac conduction defects, endocrine deficiencies, cataracts and cognitive impairments.[9] DM1 disease is caused by an unstable expansion of CTG repeats located in the 3′ untranslated region of the DM1 protein kinase (*DMPK*) gene.[10] Pathogenic expansions range from 50 to thousands of repeats; when transcribed, mutant transcripts containing expanded CUG repeats (CUGexp-RNAs) are retained in the nucleus, localizing to foci as ribonucleoprotein aggregates. Owing to their high binding affinity for repeated CUG motifs, RNA binding proteins of the MBNL family are sequestered within CUGexp-RNA foci, leading to a functional loss of MBNL proteins. This dysfunction is a major contributor to the pathogenesis of DM1, resulting in the characteristic clinical features of the disease. Notably, loss of MBNL activity reverts specific pre-mRNA processing events to a fetal pattern in affected tissues of DM1 patients. Thus, the misregulation of multiple splicing events present in DM1 skeletal and cardiac muscles has been associated with disease symptoms such as myotonia, muscle weakness, the dystrophic process and cardiac conduction defects.[11–15] Further evidence for a major role of MBNL functional loss in DM1 pathology was provided by single or combined *Mbnl* knockout (KO) mouse models that develop cardinal symptoms observed in DM1 patients.[7,8,16–20]

Although the functions of MBNL1 and MBNL2 in skeletal muscles and brain have been studied extensively, their involvement in the spinal cord and the connected peripheral nervous system remains poorly investigated. However, peripheral nerve involvement in DM1 pathophysiology has been open to debate for a long time. Indeed, several abnormalities, including abnormal motor end-plate size and arborization, were described in muscle biopsies of DM1 patients,[21–23] and additional observations suggest neuromuscular junction (NMJ) structural and functional defects in DM1.[24,25] Interestingly, spinal cord biopsies obtained from DM1 patients have shown the presence of nuclear CUGexp-RNA foci that co-localize with MBNL proteins in spinal motor neurons (MNs), possibly causing MBNL loss of function in this cell type and subsequent peripheral nerve deficiency,[26] as suggested by the aberrant splicing of CAMKK2 in MNs from DM1 patients.[27] Moreover, abnormalities of NMJs, including changes in motor end-plate size and shape, have been documented in the diaphragm muscle of DMSXL mice expressing ubiquitously large CTG repeats.[28] Likewise, altered NMJ structures were observed in the tibialis anterior (TA) muscle of *Mbnl1*$^{-/-}$; *Mbnl2*$^{+/-}$ mice, together with an increased proportion of fragmented end-plates.[7] Finally, a neuromuscular co-culture cell model combining DM1 human induced pluripotent stem cell-derived MNs and healthy muscle cells showed presynaptic defects affecting NMJ development or stability that can be reproduced by the loss of MBNL proteins in MNs.[29] Together, these observations emphasize a potential involvement of MNs in neuromuscular dysfunction and structural defects of the motor unit in DM1 but also raise a question regarding the function of MBNL proteins in the MN and their role in motor unit homeostasis via the NMJ. For this purpose, we generated MN-specific *Mbnl1; Mbnl2* conditional mice, in which *Mbnl2* expression is ablated selectively in MNs in a constitutive *Mbnl1* knockout background (MN-dKO) and demonstrated that loss of MBNL protein in MNs leads to motor unit dysfunction, which might contribute to DM1 pathogenesis.

Materials and methods

Antibodies

Rabbit monoclonal anti-synaptophysin (Syn) (Invitrogen, 1/200), polyclonal anti-neurofilament (NF) 68 kDa (Millipore Bioscience Research Reagents, 1/500) and α-bungarotoxin (α-BTX) Alexa Fluor 488 conjugate (1/500) were purchased from Invitrogen. Spinal cord immunofluorescences were performed with polyclonal anti-MBNL1 antibody (A2764, gift from C. A. Thornton, 1/1000), monoclonal anti-MBNL2 antibody (3B4, Santa Cruz, 1/300) and anti-ChAT antibody (AB144P, Millipore, 1/50).

Generation of Hb9-Cre-MN-dKO conditional knockout mice

Mbnl1$^{+/-}$:*Mbnl2LoxP/LoxP* mice[7] have been crossed with transgenic mice expressing a Cre recombinase under a MN-specific Hb9 promoter (B6.129S1-*Mnx1*^{tm}4$^{(cre)Tmj}$/J; Stock #006600, Jackson Labs) to generate Hb9-Cre-MN-dKO mice (*Mbnl1*$^{\Delta E3/\Delta E3}$, *Mbnl2*$^{c/c}$; Hb9-Cre$^{+/-}$), Hb9Cre-*Mbnl2*-KO mice (*Mbnl1*$^{+/+}$, *Mbnl2*$^{c/c}$; Hb9Cre$^{+/-}$), *Mbnl1*-KO mice (*Mbnl1*$^{\Delta E3/\Delta E3}$, *Mbnl2*$^{c/c}$; Hb9Cre$^{-/-}$) and control (CTL) mice (*Mbnl1*$^{+/+}$; *Mbnl2*$^{c/c}$; Hb9-Cre$^{-/-}$).

Animal procedures

All mouse procedures were done according to the protocols APAFIS#22706-2019110616459523v5; APAFIS#22758_201911131652 1357v8 and APAFIS#22871-2019112115405462v4 approved by the Ethical Committee on Animal Resources at the Centre Experimentation Fonctionnelle of Pitié-Salpétrière animal facility and under appropriate biological containment. Briefly, mice were maintained in a conventional specific-pathogen-free facility with a fixed light cycle (22°C, 12 h/12 h dark–light cycle). Mice have been analysed for motor function at 2 and 4 months of age by accelerating rotarod and gait analysis using Catwalk XT device.

Accelerating rotarod

Rotarod testing was performed on 2- and 4-month-old mice using the LE8200 apparatus (Harvard Apparatus). An accelerating rotarod protocol from 4 to 40 rpm over 30 s was used. The latency to fall was recorded as the mean latency of the three consecutive trials, and data are reported ± standard error of the mean (SEM).

Gait analysis

Gait analysis was performed using The CatWalk XT™ (Noldus). For data collection, six runs per animal were performed, with a minimum of three runs crossed at the same speed with three full step sequence patterns. Quantitative analysis of the data (Catwalk v.9.1 software) included the following parameters: step sequence, average speed, walking pattern, stride length, stand duration and hind–front paw distance.

In situ isometric force analysis

In situ isometric contraction of the TA muscle was performed as described previously.[30] Mice were anaesthetized by intraperitoneal injection of pentobarbitone sodium (60 mg/kg body weight). A blind analysis was performed by the investigator. The knee and foot were fixed with clamps, and the distal tendon of the TA muscle was attached using a silk ligature to a force sensor (305B, dual-mode lever, Aurora Scientific). The sciatic nerve was crushed proximally and stimulated distally by a bipolar silver electrode using supramaximal square-wave pulses of 0.1 ms duration. Muscle was also stimulated directly in order to initiate muscle contraction in the event of failure of neurotransmission. Force that was developed during isometric muscle contractions in response to nerve or muscle tetanic stimulation (frequency of 100 Hz, train of stimulation of 500 ms) was then measured. The maximal absolute force was determined at optimal length (i.e. length at which supramaximal tension was obtained during the tetanus). Signals from the force sensor were amplified and digitized with a computer equipped with an analog-to-digital interface board (Powerlab, ADInstruments) using LabChart v.8 software (ADInstruments). Myotonia was quantified as the area beneath the curve of muscle force decaying over time after stimulation. After recordings, the mice were euthanized by cervical dislocation and the muscles harvested.

RNA extraction and RNA sequencing

Total RNAs from the entire cross-section of the L3–L6 segments of the lumbar spinal cord from 4-month-old mice ($n = 4$ mice per condition) were isolated using TRI-Reagent® (Sigma-Aldrich) according to the manufacturer's protocol, and tissues were lysed using Fastprep system and Lysing Matrix D tubes (MP biomedicals). Total stranded RNA sequencing was performed at the Platform of the Institut du Cerveau. RNA quality control of each sample was realized with Tapestation 2200 (Agilent), and libraries were prepared with the KAPA mRNA hyperprep Roche kit, from an input of 250 ng. Sequencing was performed on an Illumina NovaSeq 6000 as paired-end 150 bp reads with a sequencing depth of 140 million reads. Sequence data quality was assessed using FastQC and MultiQC tools, and RNA-sequencing reads were trimmed using Cutadapt (v.2.10) and aligned with STAR (v.2.7.5a). The reference genomes used for the alignment were *Mus musculus* (house mouse) genome assembly GRCm38 (mm10). Quantification of transcripts followed with HTSeq (v.0.12.4). All the steps were built in a Nextflow (v.20.04.1) pipeline. Differential gene expression analysis was performed using DESeq2 [false discovery rate (FDR) < 0.05; $\log_2$ fold-change > 1], and differential alternative splicing was detected by rMATS (v.4.1.2) (FDR corrected $P < 0.05$, delta per cent spliced in (ΔPSI) ≥ 10%), using the STAR-aligned files as input (.bam). Detection of events was done with a 'prep' step of each pair of conditions (CTL versus MN-dKO, CTL versus *Mbnl1*-KO, CTL versus Hb9Cre-*Mbnl2*-KO), a 'post' step of all conditions together, and finally, a 'stats' step of each pair of conditions to define *pvalue*, *FDR* and *IncLevelDifference* for each comparison. Analysis of GO terms and biological pathways enrichment was done by combining EnrichR[31,32] (GO Biological process[33,34]) and HemI v.2.0 for visualization.[35]

Reverse transcription PCR

Two hundred nanograms of RNA was reverse transcribed using SuperScriptIV™ first-strand synthesis system (Life Technologies) in a total of 20 µL. The complementary DNA (0.5 µL) was subsequently used in a semi-quantitative PCR analysis according to the standard protocol (ReddyMix, ThermoFisher). PCR amplification was carried out for 0–35 cycles for splicing of pre-mRNA within the linear range of amplification for each gene. PCR products were quantified using the QIAxcel Advanced system (Qiagen). Tanc2 ex 23a and Cacna1d ex 12a primers were as described by Charizanis *et al.*[16] Clasp1 ex26 was described by Dinca *et al.*[36] Dvl1 ex 14b primers were ex13FW (CTTACCAGGACCCTGGCTTC) and ex15REV (TGATTCACTGCCACTACCCC).

Staining of NMJ from isolated muscle fibres

The TA muscle fibres from adult 2- and 4-month-old mice were dissected, fixed with 4% paraformaldehyde in phosphate buffered saline (PBS) for 1 h and rinsed with PBS at room temperature before storage at 4°C. Isolated muscle fibres were then stained as described previously.[37] Briefly, isolated muscle fibres were washed three times for 15 min in PBS, incubated for 15 min with 100 mM glycine in PBS, permeabilized (0.5% Triton X-100 in PBS) for 1 h and blocked for 4 h in blocking buffer (3% bovine serum albumin, 5% goat serum and 0.5% Triton X-100 in PBS). Isolated muscle fibres were incubated overnight at 4°C with rabbit polyclonal antibodies against neurofilament (NF) 68 kDa and synaptophysin (Syn) in blocking solution. After three washes in PBS, muscles were incubated overnight at 4°C with Alexa Fluor 555 goat anti-rabbit IgG and Alexa Fluor 488-conjugated α-BTX in blocking solution. After three washes in PBS, isolated muscle fibres were flat mounted in Vectashield (Vector Laboratories) mounting medium. Images of at least $n =$ 15 NMJs per mouse were collected with Zeiss LSM880 confocal microscope and processed through a semi-automatic ImageJ macro adapted from NMJS-morph.[38]

Spinal cord Nissl staining

Anaesthetized mice were perfused transcardially with PBS, followed by 4% paraformaldehyde in phosphate buffer for fixation. spinal cords were post-fixed in 4% paraformaldehyde overnight, cryoprotected in 30% sucrose for >24 h and embedded in Tissue-Tek before storage at −80°C. Transverse cryosections (14 µm thick) of lumbar spinal cords were mounted on slides, air dried for 30 min and stored at −80°C until staining. Slides were air dried for 30 min, then rinsed in 70% ethanol for 1 min, stained with Cresyl Violet (0.05% glacial acid acetic and 0.05% Cresyl Violet in distilled water) for 15 min, then quickly rinsed in several ethanol baths (70%, 70%, 90% and 100%) before dehydration with xylene for 1 min. Sections were covered in DPX mounting medium, then coverslipped before drying overnight.

Spinal cord immunostaining

MN immunostaining was adapted from Besse *et al.*[39] After air drying for 30 min, slides with transverse cryosections of lumbar spinal cords were permeabilized for 30 min (0.1% Triton X-100 in PBS). Then, we performed an unmasking procedure using 85°C heated citric acid monohydrate (10 mM, pH 6), incubating slides in it twice for 5 min. Sections were then cooled in cold PBS. Sections were then washed using the following procedure, repeated throughout the experiment: twice in PBS for 5 min, then in 0.1% Triton X-100 in PBS for 2 min and once again in PBS for 5 min. Sections were isolated using Dako pen. Sections were blocked for 1 h in blocking buffer (4% bovine serum albumin, 10% donkey serum and 0.1% Triton X-100 in PBS), then incubated with anti-MBNL1, anti-MBNL2 and anti-ChAT antibodies overnight at 4°C in the blocking solution. Sections were washed, then incubated for 1 h at room temperature with Alexa fluor Alexa Fluor 488 donkey anti-rabbit IgG, Alexa Fluor 555 donkey anti-mouse IgG and Alexa Fluor 647 donkey anti-goat IgG in 0.1% Triton X-100 in PBS. Finally, sections were washed, incubated with Hoechst (1/2500 in PBS) for 10 min, washed twice with PBS and flat mounted in Vectashield (Vector Laboratories) mounting medium. Images were obtained using a Nikon Ti2 confocal microscope with a SCU-W1 spinning disk head (Yokogawa).

Transmission electron microscopy

Mouse TA were fixed for 2 h with 2% paraformaldehyde and 2% glutaraldehyde in 0.1 M phosphate buffer (pH 7.4). Samples were post-fixed with 2% OsO_4, in 0.1 M phosphate buffer (pH 7.4) for 1 h, then dehydrated in a graded series of acetone, including a 1% uranyl acetate staining step in 70% acetone, and finally embedded in epoxy resin (EMBed-812, Electron Microscopy Sciences, USA). Ultra-thin (70 nm) sections were stained with uranyl acetate and lead citrate, examined using a CM100 Philips transmission electron microscope and photographed with a digital SIS Morada camera.

Statistical analysis

All statistical analyses were performed using the GraphPad Prism software (v.8, GraphPad Software Inc.). Data distribution was assessed by the Shapiro–Wilk test prior to the use of one-way ANOVA as appropriate.

Results

MBNL depletion affects locomotion

To examine the function of MBNL1 and MBNL2 in the MN on motor unit homeostasis, we generated conditional MN-specific *Mbnl2*-KO mice, in which *Mbnl2* expression is ablated selectively from spinal MNs using the homeobox gene 9 (Hb9) promoter to drive Cre recombinase expression.[40–46] We investigated the consequence of specific *Mbnl2* depletion in MNs with or without *Mbnl1* being constitutively null (Fig. 1A). The MN-dKO mice are developmentally viable and do not display overt disease-associated phenotypes at early postnatal ages. Adult 2- and 4-month-old MN-dKO mice have a comparable body weight to adult Hb9Cre-*Mbnl2*-KO, *Mbnl1*-KO ($Mbnl1^{-/-}$; Hb9Cre-$Mbnl2^{+/+}$) and CTL ($Mbnl1^{+/+}$; Hb9Cre-$Mbnl2^{+/+}$) mice (Supplementary Fig. 1A and B). To evaluate Cre recombinase efficiency in MNs, we examined MBNL2 protein expression in the spinal cord. As expected, MBNL1 protein was not observed in any cells of the spinal cord in MN-dKO mice, and MBNL2 protein was absent from choline acetyltransferase (ChAT)-positive cells in MN-dKO mice, confirming efficient Cre recombination (Supplementary Fig. 1C). Quantification of MN viability by Nissl staining in the ventral horn of spinal cord sections of 4-month-old animals did not reveal a significant difference in the number of MNs from *Mbnl1*-KO, Hb9Cre-*Mbnl2*-KO or MN-dKO mice compared with CTL mice, indicating that MBNL1 and MBNL2 are not required for MN survival (Supplementary Fig. 1D and E).

Although adult Hb9Cre-*Mbnl2*-KO mice did not develop overt phenotypes and were indistinguishable from CTL mice, *Mbnl1*-KO and MN-dKO mice gradually developed abnormal motor behaviours and showed impaired rotarod performances (Supplementary Fig. 2). Gait analysis confirmed that 2-month-old *Mbnl1*-KO and MN-dKO mice exhibited reduced mobility with a comparable average speed reduction for both genotypes compared with CTL mice (Fig. 1B, Supplementary Videos 1–4 and Supplementary Fig. 3A). Of interest, the coordination patterns of walking were significantly different in 2-month-old MN-dKO mice compared with *Mbnl1*-KO and CTL mice, with a reduced percentage of the classical diagonal limb walking pattern and a preferential use of other patterns of walking (three, four limbs and alternative walking patterns) (Fig. 1C). These modifications are associated with an increase of the front/hind pawprint mean intensity ratio, indicative of impaired balance in MN-dKO mice (Fig. 1D). Additional analysis of interlimb coordination parameters showed a shorter stride length of the front and hind legs in *Mbnl1*-KO and MN-dKO mice compared with CTL mice (Fig. 1E), in addition to a larger distance between the position of the hind paw and the position of the previously placed front paw on the same side of the body (Fig. 1G). However, there was no significant modification of the stand duration (also known as stance duration) or the swing duration, suggesting a complex interplay of factors influencing mouse locomotion (Fig. 1F and Supplementary Fig. 3B and C).

We next examined the effect of MBNL1 and MBNL2 loss in the MNs on skeletal muscle homeostasis. Initially, histological analysis from the TA muscle of 2-month-old mice did not show the presence of central nuclei in myofibres, a DM1 feature, from *Mbnl1*-KO and MN-dKO mice (Fig. 2A). However, *in situ* force measurements confirmed the presence of myotonia in *Mbnl1*-KO and MN-dKO mice (Fig. 2B). Importantly, a 30% reduction of specific maximal force in response to tetanic sciatic nerve stimulation was observed only in MN-dKO mice compared with CTL animals (Fig. 2C). Thus, the combined loss of MBNL1 and MBNL2 in MNs leads to early coordination defects and muscle weakness.

Given that we observed a progressive alteration in the ambulatory behaviour of mice with age, we analysed 4-month-old *Mbnl*-KO mice. (Supplementary Videos 5–8). Analysis of the walking patterns and coordination parameters of *Mbnl1*-KO and MN-dKO mice showed an aggravation, with comparable gait

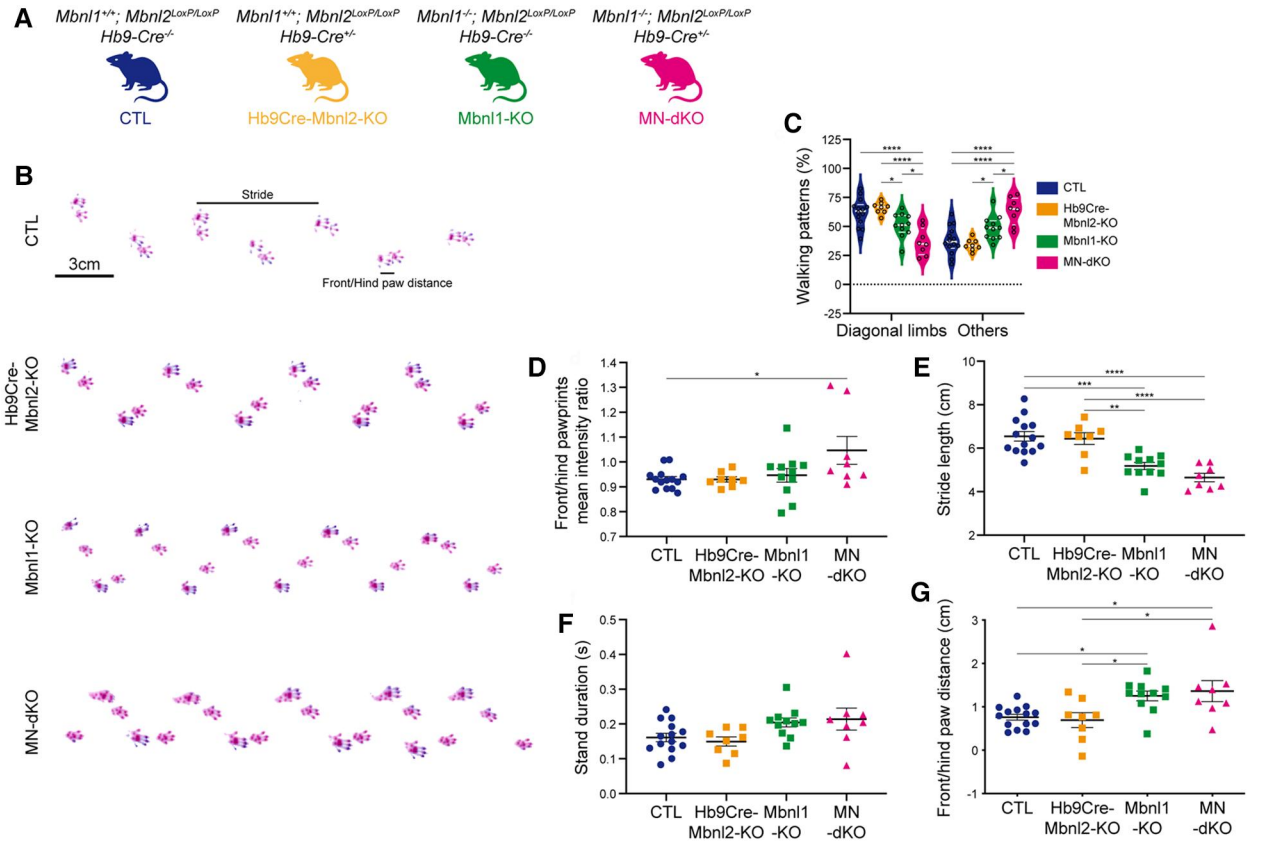

Figure 1 MBNL1 and MBNL2 combined depletion in motor neurons affects mouse coordination. (**A**) Schematic representation of the breeding strategy used to deplete MBNL2 specifically in motor neurons (MNs) in transgenic mice. *Mbnl1*$^{+/-}$; *Mbnl2*$^{LoxP/LoxP}$ mice were crossed with Mxn1Cre mice (also known as Hb9Cre mice) to generate: *Mbnl1*$^{+/+}$; Hb9-*Mbnl2*$^{+/+}$ control mice (CTL); *Mbnl1*$^{-/-}$; Hb9-*Mbnl2*$^{-/-}$ MN-dKO mice; *Mbnl1*$^{-/-}$; Hb9-*Mbnl2*$^{+/+}$ *Mbnl1*-KO mice; and *Mbnl1*$^{+/+}$; Hb9-*Mbnl2*$^{-/-}$ Hb9Cre-*Mbnl2*-KO mice. (**B**) Representative trace of footprint analysis for testing gait abnormalities in CTL, HB9Cre-*Mbnl2*-KO, *Mbnl1*-KO and MN-dKO mice at 2 months of age. (**C–G**) Quantification from the gait analyses for 2-month-old CTL, HB9Cre-*Mbnl2*-KO, *Mbnl1*-KO and MN-dKO mice. (**C**) Proportions of walking patterns, defined by the limbs mice are standing on at the same time during walking. 'Others' refers to standing on three or four limbs, and alternative walking patterns. (**D**) Ratio of the mean intensity of pixels corresponding to front leg pawprints on the mean intensity of pixels corresponding to hind leg pawprints. (**E**) Quantification of the mean stride length of all paws. (**F**) Quantification of the mean standing time of all paws. (**G**) Quantification of front/hind paw distance of either ipsilateral combination of paws. Data are mean ± standard error of the mean from 2-month-old $n_{CTL} = 14$; $n_{Hb9Cre\text{-}Mbnl2\text{-}KO} = 8$; $n_{Mbnl1\text{-}KO} = 11$; $n_{MN\text{-}dKO} = 8$ mice. $^{*}P < 0.05$, $^{**}P < 0.01$, $^{***}P < 0.001$ and $^{****}P < 0.0001$; Tukey's test. dKO = double knockout; MN = motor neuron.

modifications observed between the two genotypes compared with CTL mice (Fig. 3 and Supplementary Fig. 3D–F). However, only 4-month-old MN-dKO mice developed a significant increase of the stand duration compared with CTL mice, indicating further impairment in gait stability or coordination (Fig. 3E). At the skeletal muscle level, TA muscle histological analysis showed the presence of central nuclei in myofibres from *Mbnl1*-KO and MN-dKO mice (Fig. 4A), with no modification of the proportion of centronucleated fibres in MN-dKO compared with *Mbnl1*-KO mice (Fig. 4B). *In situ* force measurements confirmed the presence of myotonia in *Mbnl1*-KO mice, with a decrease of specific maximal force in response to tetanic sciatic nerve stimulation compared with CTL, as previously reported.[47,48] Likewise, MN-dKO mice exhibited myotonia and a reduced specific maximal force compared with CTL, which are comparable to *Mbnl1*-KO mice (Fig. 4C and D).

Thus, MBNL1 loss leads to progressive motor deficiencies, but aggravated coordination defects and muscle specific force reduction arise precociously from the loss of both MBNL1 and MBNL2 in MNs. These results suggest that MBNL1 and MBNL2 might be involved in the anterograde regulation of motor coordination and function.

MBNL proteins are involved in neuromuscular junction maintenance

Given that locomotion requires interplay between MNs and skeletal muscle through the NMJ, we analysed its morphology in isolated TA fibres from *Mbnl1*-KO, Hb9Cre-*Mbnl2*-KO, MN-dKO and CTL mice. At 2 months of age, NMJs from TA from Hb9Cre-*Mbnl2*-KO and *Mbnl1*-KO mice were innervated and exhibited a typical mature 'pretzel-like' shape (Fig. 5A). Quantitative analyses showed that acetylcholine receptor (AChR) cluster area, nerve terminal area, end-plate perimeter and postsynaptic fragmentation of NMJs of Hb9Cre-*Mbnl2*-KO and *Mbnl1*-KO were similar to CTL mice (Fig. 5B–F). Interestingly, NMJs of 2-month-old MN-dKO mice adopted a characteristic 'pretzel-like' shape, with an enlarged AChR cluster area, nerve terminal area and motor end-plate perimeter compared with CTL and *Mbnl1*-KO mice (Fig. 5B–D). In addition, NMJ postsynaptic structures in the TA from MN-dKO mice were discontinuous (Fig. 5A). Quantitative analysis showed an increase of AChR cluster fragmentation in NMJs of MN-dKO mice compared with *Mbnl1*-KO mice (Fig. 5E), with a decrease of 30% of NMJs containing one to three AChR clusters and an increase of NMJs containing more than four fragments (Fig. 5F). Despite this change, the overlap ratio between

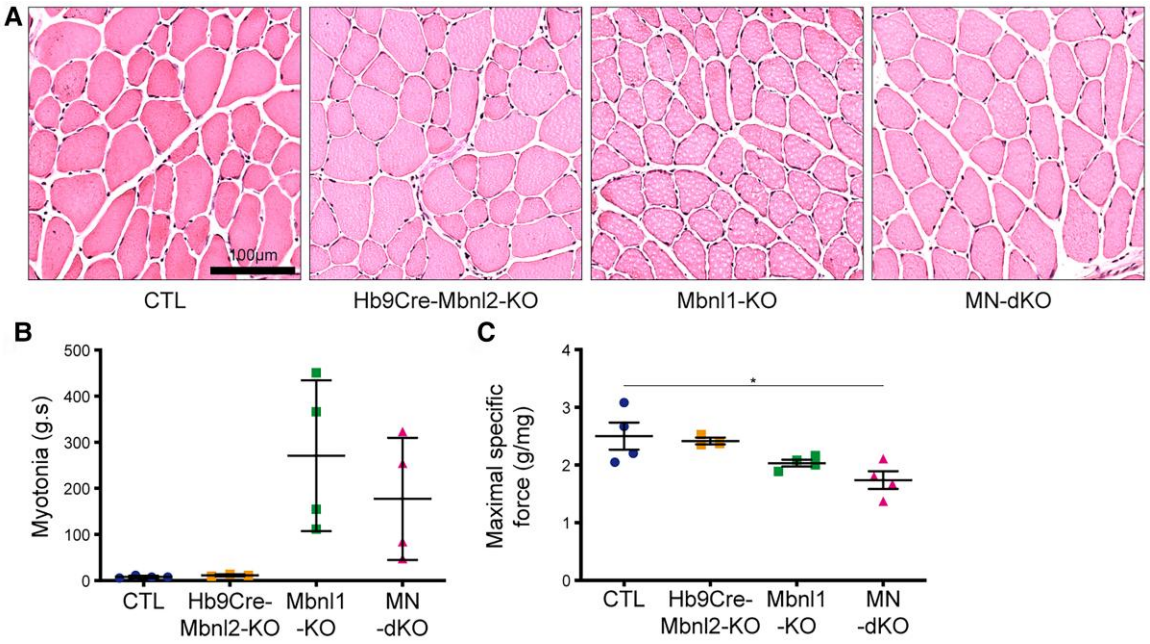

Figure 2 MBNL1 and MBNL2 combined depletion in motor neurons leads to early mouse muscle strength reduction. Analysis of tibialis anterior muscles from 2-month-old control (CTL), Hb9Cre-*Mbnl2*-KO, *Mbnl1*-KO and MN-dKO mice. (**A**) Haematoxylin and eosin staining of tibialis anterior cryosections. Scale bar = 100 µm. (**B**) *in situ* measurement of myotonia (in grams seconds). (**C**) Tibialis anterior *in situ* muscle maximal specific force (in grams per milligram). Data are mean ± standard error of the mean from 2-month-old mice: $n_{CTL} = 4$; $n_{Hb9Cre\text{-}Mbnl2\text{-}KO} = 3$; $n_{Mbnl1\text{-}KO} = 4$; $n_{MN\text{-}dKO} = 4$ mice. $^{*}P < 0.05$; one-way ANOVA, Tukey's test. dKO = double knockout; MN = motor neuron.

presynaptic and postsynaptic markers, connotative of NMJ innervation, remained unchanged in Hb9Cre-*Mbnl2*-KO, *Mbnl1*-KO and MN-dKO mice compared with CTL mice (Fig. 5G). These observations were confirmed in soleus muscles, with enlarged nerve terminal areas and end-plate perimeters in MN-dKO mice compared with CTL mice (Supplementary Fig. 4). However, contrary to TA muscles, NMJ postsynaptic structures were discontinuous with AChR cluster fragmentation in NMJs of both *Mbnl1*-KO and dKO mice (Supplementary Fig. 4E), with a decrease of 40% of NMJs containing one to three AChR clusters and an increase of NMJs containing more than four fragments (Supplementary Fig. 4F).

These observations suggest that loss of either MBNL1 or MBNL2 in MNs does not impair NMJ innervation or development (formation and maturation), whereas depletion of both MBNL proteins alters NMJ morphological features.

To determine whether the loss of MBNL proteins is crucial for NMJ maintenance, we analysed NMJs of TA and soleus muscles from older CTL and *Mbnl*-KO mice (Fig. 6 and Supplementary Fig. 5). At 4 months of age, NMJs of Hb9Cre-*Mbnl2*-KO mice resembled NMJs of CTL mice (Fig. 6), as observed at 2 months of age. However, AChR clusters of *Mbnl1*-KO mice were larger, with an increased AChR cluster area and end-plate perimeter, whereas in MN-dKO mice these parameters were similar to CTL mice (Fig. 6B and C). Also, the area of presynaptic nerve terminal remained unchanged between genotypes (Fig. 6D). Nevertheless, TA muscle NMJs of *Mbnl1*-KO and MN-dKO mice exhibited severe AChR cluster fragmentation, with a decrease of 40% of NMJs containing one to three fragments and appearance of >30% of MN-dKO NMJs containing seven fragments or more compared with CTL mice (Fig. 6E and F). These deficits were associated with reduced pre- and postsynaptic overlap ratio in *Mbnl1*-KO and MN-dKO mice compared with CTL mice (Fig. 6G and Supplementary Fig. 6A). Of interest, NMJs of TA muscles from MN-dKO mice exhibited abnormal nerve terminal sprouts (short axonal extensions beyond innervated AChR clusters) without any co-localization with AChR clusters (Fig. 6A, arrowhead, Fig. 6H and Supplementary Fig. 6B), suggesting the occurrence of synaptic plasticity changes that might originate from MNs.

Transmission electron microscopy of NMJs of 4-month-old mice support these observations. In *Mbnl1*-KO mice, ultrastructural abnormalities were restricted to the postsynaptic area of NMJs, with enlarged synaptic gutters, irregularly shaped crests and the presence of degenerative structures. In contrast, NMJs of MN-dKO mice not only reproduced postsynaptic alterations seen in *Mbnl1*-KO mice but also developed presynaptic defects, such as degenerative structures inside the presynaptic boutons and partial denervation (Fig. 7). The occurrence of synaptic remodelling was also suggested by the presence of non-myelinating terminal Schwann cells processes extending into the synaptic cleft of MN-dKO mouse NMJs, which are known to restrict ACh diffusion and impact nerve transmission (Supplementary Fig. 6C). Our results show specific presynaptic modifications of NMJs in MN-dKO mice only, highlighting the deleterious effect of a combined loss of MBNL1 and MBNL2 in MNs. Progressive disruption of NMJ structures between 2 and 4 months of age in *Mbnl1*-KO and MN-dKO mice also supports a role for MBNL1 and MBNL2 in NMJ maintenance (Supplementary Table 1). While analysing both slow-twitch soleus muscles and fast-twitch TA muscles, we observed similar modifications of NMJ structures in both muscle types. This suggests that the NMJ structural characteristics we studied are consistent across different muscle fibre types in *Mbnl1*-KO and MN-dKO mice. These findings indicate that the alterations in NMJ structure are not restricted to a specific muscle type but are a general feature observed in the *Mbnl* model.

However, the presence of presynaptic structural and ultrastructural abnormalities solely in the NMJs of MN-dKO mice suggests that MBNL proteins in MNs might regulate fine processes involved in nerve to muscle communication, muscle strength and locomotor coordination.

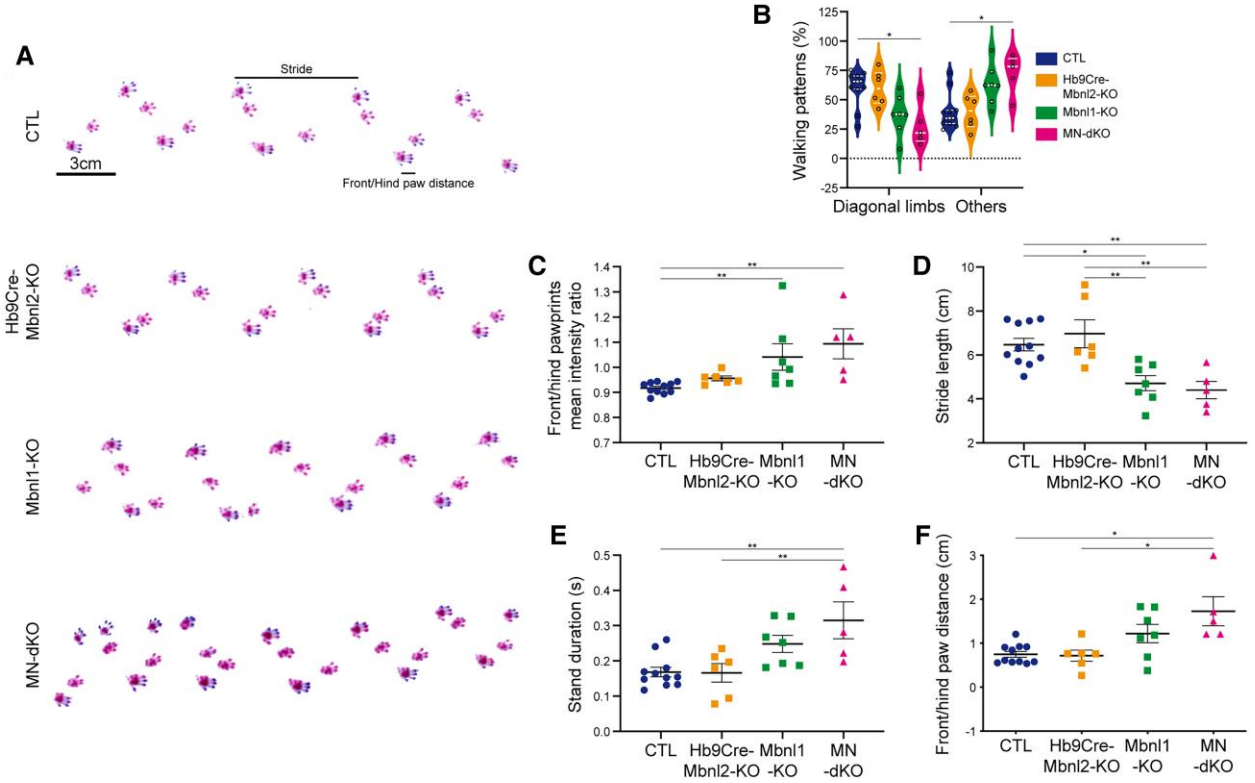

Figure 3 Progressive worsening of *Mbnl1*-KO and MN-dKO locomotor abilities. (**A**) Representative trace of footprint analysis for testing gait abnormalities in control (CTL), Hb9Cre-*Mbnl2*-KO, *Mbnl1*-KO and MN-dKO mice at 4 months of age. (**B–F**) Quantification from the gait analyses for 2-month-old CTL, HB9Cre-*Mbnl2*-KO, *Mbnl1*-KO and MN-dKO mice. (**B**) Proportions of walking patterns, defined by the limbs mice are standing on at the same time during walking. 'Others' refers to standing on three or four limbs, and alternative walking patterns. (**C**) Ratio of the mean intensity of pixels corresponding to front leg pawprints on the mean intensity of pixels corresponding to hind leg pawprints. (**D**) Quantification of the mean stride length of all paws. (**E**) Quantification of the mean standing time of all paws. (**F**) Quantification of front/hind paw distance of either ipsilateral combination of paws. Data are mean ± standard error of the mean from 4-month-old mice: $n_{CTL} = 11$; $n_{Hb9Cre\text{-}Mbnl2\text{-}KO} = 6$; $n_{Mbnl1\text{-}KO} = 7$; $n_{MN\text{-}dKO} = 5$ mice. $^{*}P < 0.05$, $^{**}P < 0.01$; one-way ANOVA, Dunn's test (**B**, **C** and **F**); one-way ANOVA, Tukey's test (**D** and **E**). dKO = double knockout; MN = motor neuron.

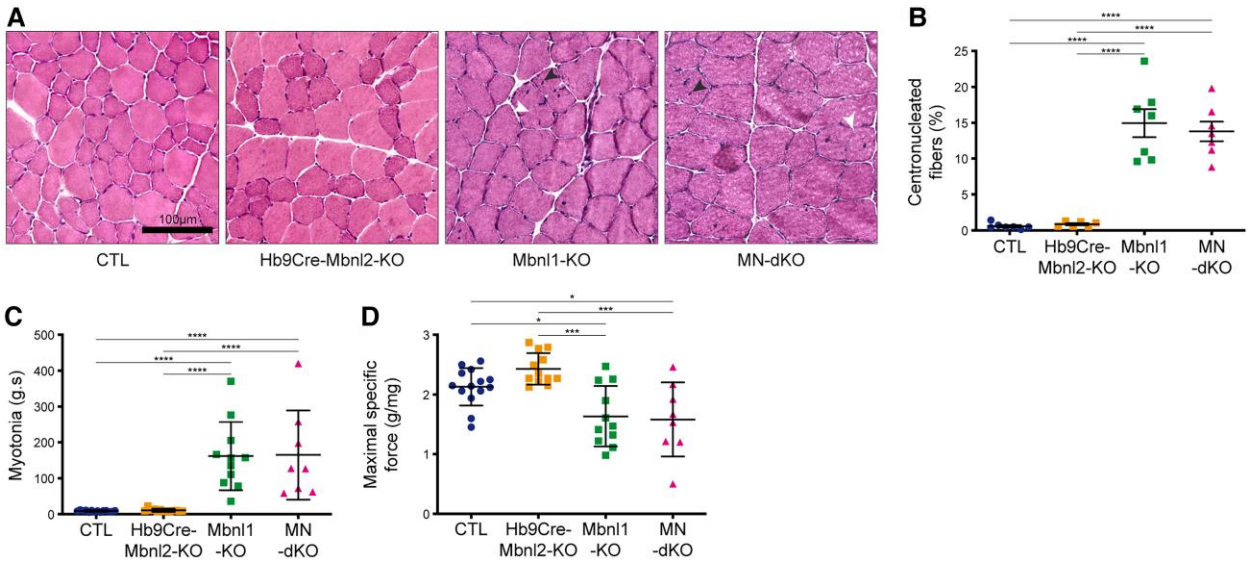

Figure 4 Progressive muscle histology and strength modifications in *Mbnl1*-KO and MN-dKO mice. Analysis of tibialis anterior muscles from 4-month-old control (CTL), Hb9Cre-*Mbnl2*-KO, *Mbnl1*-KO and MN-dKO mice. (**A**) Haematoxylin and eosin staining of tibialis anterior cryosections. White arrows = split fibres; black arrows = centronucleated fibres. Scale bar = 100 µm. (**B**) Proportions of centronucleated fibres in tibialis anterior muscle transverse cryosections. (**C**) *In situ* measurement of myotonia (in grams seconds). (**D**) Tibialis anterior *in situ* muscle maximal specific force (in grams per milligram). Data are mean ± standard error of the mean from 4-month-old mice: $n_{CTL} = 7$; $n_{Hb9Cre\text{-}Mbnl2\text{-}KO} = 6$; $n_{Mbnl1\text{-}KO} = 7$; $n_{MN\text{-}dKO} = 7$ mice (**B**); and $n_{CTL} = 14$; $n_{Hb9Cre\text{-}Mbnl2\text{-}KO} = 12$; $n_{Mbnl1\text{-}KO} = 11$; $n_{MN\text{-}dKO} = 8$ mice (**C** and **D**). $^{*}P < 0.05$, $^{***}P < 0.001$ and $^{****}P < 0.0001$; one-way ANOVA, Tukey's test. dKO = double knockout; MN = motor neuron.

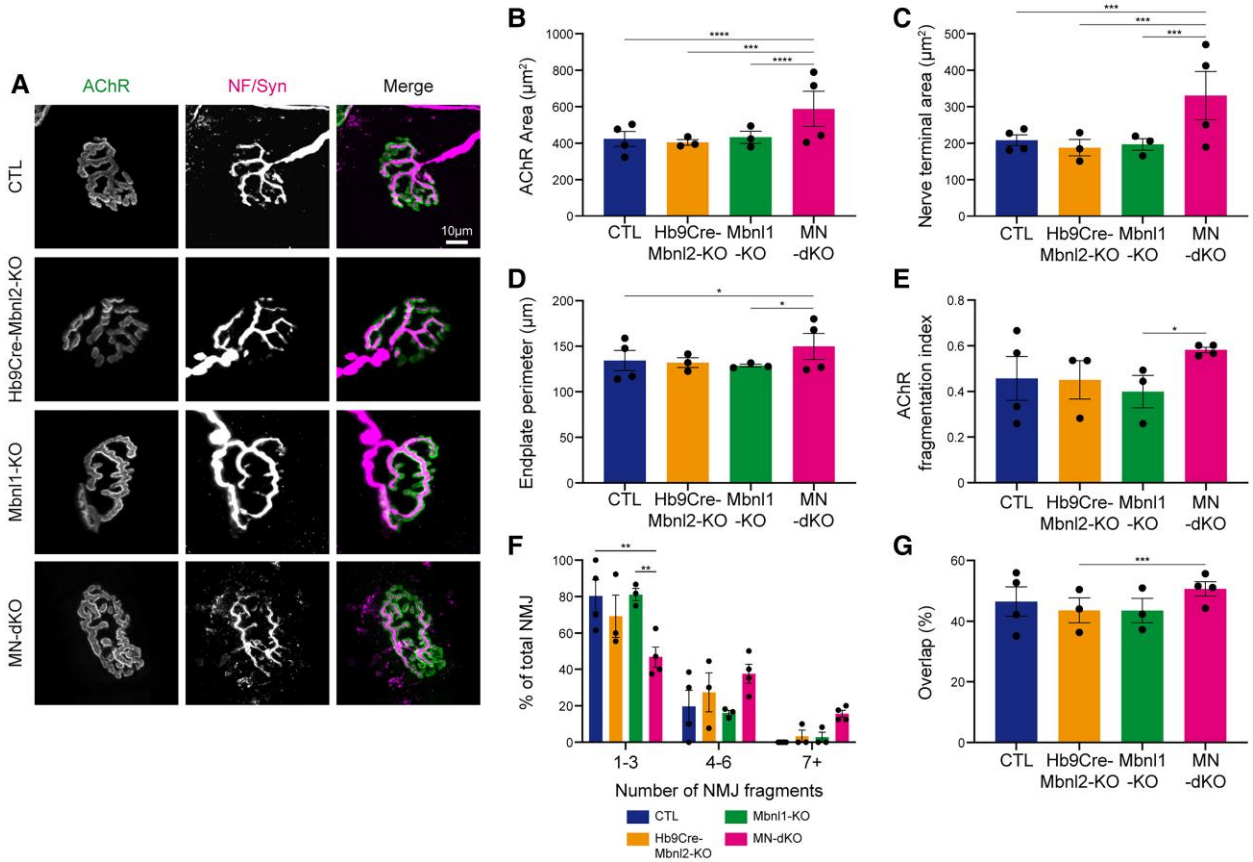

Figure 5 MN-dKO mice exhibit neuromuscular junction structural alterations at 2 months of age. (**A**) Representative confocal images of isolated muscle fibres from 2-month-old control (CTL), Hb9Cre-*Mbnl2*-KO, *Mbnl1*-KO and MN-dKO tibialis anterior muscle stained with antibodies to neurofilament (NF) and synaptophysin (Syn, magenta) together with α-bungarotoxin (α-BTX; AChR, green), with quantitative analysis in **B–G**. (**B**) AChR cluster area. (**C**) Neuromuscular junction (NMJ) nerve terminal area. (**D**) End-plate perimeter. (**E**) Index of AChR fragmentation. **(F)** Percentages of NMJs that contain indicated numbers of AChR fragments. (**G**) Overlap ratio of pre- and postsynaptic AChR cluster area staining. Data are mean ± standard error of the mean from $n_{CTL} = 4$; $n_{Hb9Cre\text{-}Mbnl2\text{-}KO} = 3$; $n_{Mbnl1\text{-}KO} = 3$; $n_{MN\text{-}dKO} = 4$. $^{*}P < 0.05$, $^{**}P < 0.01$, $^{***}P < 0.001$ and $^{****}P < 0.0001$; one-way ANOVA, Dunn's test (**B**, **E** and **G**); one-way ANOVA, Tukey's test (**C** and **D**); and two-way ANOVA, Tukey's test (**F**). dKO = double knockout; MN = motor neuron.

MBNL proteins in motor neurons regulate alternative splicing of RNAs involved in synaptic neurotransmission

To explore the molecular consequences of MBNL1 and MBNL2 loss in MNs, we performed high-throughput RNA sequencing using total RNA isolated from lumbar spinal cord of MN-dKO and CTL 4-month-old mice. Differential gene expression analysis using DESeq2 (FDR < 0.05; $\log_2$ fold change ≥ 1) did not reveal overt gene expression changes in spinal cord from MN-dKO mice compared with CTL mice, with only 48 genes that were significantly misregulated (Supplementary Table 2).

Given that MBNL proteins are known to be key regulators of RNA metabolism such as alternative splicing in mammals, we explored the impact of MBNL1 and MBNL2 deficiencies on spinal cord pre-mRNA processing and performed rMATS analysis (Supplementary Tables 3–5). Comparison of MN-dKO and CTL mice revealed 1017 differential alternative splicing events (DSE), affecting 815 unique genes [FDR corrected $P < 0.05$, delta per cent spliced in (ΔPSI) ≥ 10%], with a majority of skipped exon (SE) events (68.9%) (Fig. 8A). A majority of DSE (65%) are between 10% and 20%, with a median 17% ΔPSI value. Gene ontology (GO) biological process analysis of these 815 differentially alternative spliced RNAs showed top categories involved in microtubule cytoskeleton organization, NMJ development and neurotransmitter exocytosis (Fig. 8B). DSE analysis outlined already documented MBNL1 RNA targets in the CNS, including Clasp1 exon 26, Clasp2 ex16, Dnm2 exon 10 and Mapt exon 3, in addition to MBNL2 RNA targets, including Tanc2 ex23a, St3gal3 ex3, Csnk1d ex9 and Dlg2 ex17b (Fig. 8C). To support this computational analysis, we performed reverse transcriptase (RT)-PCR assays on CTL and MN-dKO lumbar spinal cord RNA and confirmed significant changes of Tanc2, Clasp1 and Cacna1d (Supplementary Fig. 7A). Comparison of MN-dKO and *Mbnl1*-KO mice revealed 660 DSE (FDR corrected $P < 0.05$, ΔPSI ≥ 10%), with a majority of SE (63.8%) and 104 DSE already found in *Mbnl1*-KO mice (compared with CTL), showing a greater difference in MN-dKO mice, in accordance with MBNL1 and MBNL2 compensatory effects (Supplementary Table 2).

Among DSE relevant to MN synaptic neurotransmission and associated with NMJs, we noticed an aberrant inclusion of Dvl1 39 bp exon 14b only in spinal cord from MN-dKO mice (Fig. 8D). We validated this observation by RT-PCR and confirmed a significant increased inclusion of this 39 bp exon only in MN-dKO mice (Fig. 8E). To determine the respective contributions of MBNL1 and MBNL2 loss to DSE observed in MN-dKO mice, we compared them with DSE in *Mbnl1*-KO and Hb9Cre-*Mbnl2*-KO (compared with CTL) mice (Fig. 8F). Hierarchical clustering revealed

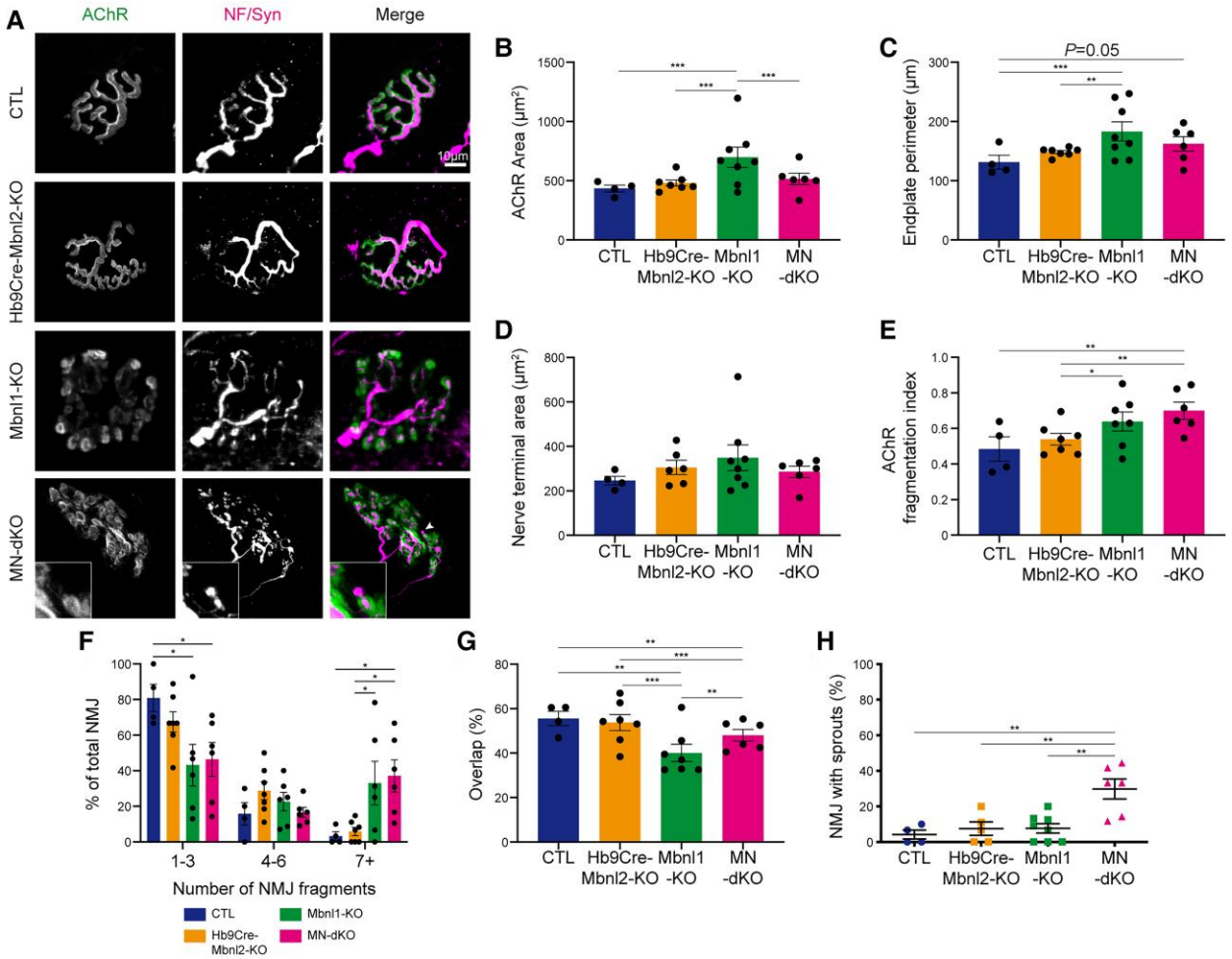

Figure 6 Aggravation of neuromuscular junction structural alterations in *Mbnl1*-KO and MN-dKO mice with age. (**A**) Representative confocal images of isolated muscle fibres from 4-month-old control (CTL), Hb9Cre-*Mbnl2*-KO, *Mbnl1*-KO and MN-dKO tibialis anterior muscle stained with antibodies to neurofilament (NF) and synaptophysin (Syn, magenta) together with α-bungarotoxin (α-BTX; AChR, green), with quantitative analysis in **B–H**. (**B**) AChR cluster area. (**C**) Neuromuscular junction (NMJ) nerve terminal area (**D**) End-plate perimeter. (**E**) Index of AChR fragmentation. (**F**) Percentages of NMJs that contain indicated numbers of AChR fragments. (**G**) Overlap ratio of pre- and postsynaptic AChR cluster area staining. (**H**) Proportion of NMJs with nerve terminal sprouts (indicated in **A** with a white arrow and magnified in the left bottom corner). Data are mean ± standard error of the mean from $n_{CTL} = 4$; $n_{Hb9Cre\text{-}Mbnl2\text{-}KO} = 7$; $n_{Mbnl1\text{-}KO} = 7$; $n_{MN\text{-}dKO} = 6$. *$P < 0.05$, **$P < 0.01$ and ***$P < 0.001$; one-way ANOVA, Tukey's test (**H**); one-way ANOVA, Dunn's test (**B–E** and **G**); and two-way ANOVA, Tukey's test (**F**). dKO = double knockout; MN = motor neuron.

that spinal cords of MN-dKO mice have a distinct RNA splicing profile compared with CTL, *Mbnl1*-KO and HB9Cre-*Mbnl2*-KO mice (Supplementary Fig. 7B). GO top categories from DSE common to *Mbnl1*-KO and MN-dKO mice highlight endocytosis (comprising synaptic vesicle endocytosis) and cytoskeleton organization (Fig. 8G), while GO analysis from DSE common to Hb9Cre-*Mbnl2*-KO and MN-dKO mice show enriched pathways in synaptic vesicle regulation, revealing specific involvement in neurotransmitter secretion, glutamatergic synaptic transmission, RNA transport and synaptic plasticity (Fig. 8H). Altogether, our data indicate that MBNL1 and MBNL2 regulate different processes in MNs to fine-tune synaptic transmission to skeletal muscle through the NMJ.

Discussion

Our data reveal the importance of MBNL1 and MBNL2 proteins in the maintenance of NMJs and suggest a role for these two proteins in regulating the synaptic transmission from MNs to skeletal muscle. MBNL protein functions in the CNS have been studied extensively and have documented a major role of MBNL2 in neuronal cells.[16,17] Our RNA splicing analysis on spinal cords from MN-dKO mice revealed that MBNL1 and MBNL2 regulate neurotransmission in MNs by targeting transcripts involved in synaptic vesicle homeostasis, neurotransmitter release and RNA localization. Additionally, MBNL proteins are known to play a crucial role in mRNA localization and transport.[49,50] Several mechanisms, including RNA transport alterations attributable to modifications of alternative last exons, impairments in mRNA transport and synaptic vesicles along microtubules, could contribute collectively to modifications in local translation and neurotransmission.

Moreover, we also confirmed the importance of MBNL proteins for NMJ function. Among DSE identified in the spinal cord from MN-dKO mice, we uncovered a number of mis-splicing events previously reported in the brain of *Mbnl*-KO mice.[16,17,51] A set of pre-mRNAs are regulated in a similar manner by MBNL1 and MBNL2 in both the brain and spinal cord, suggesting that similar

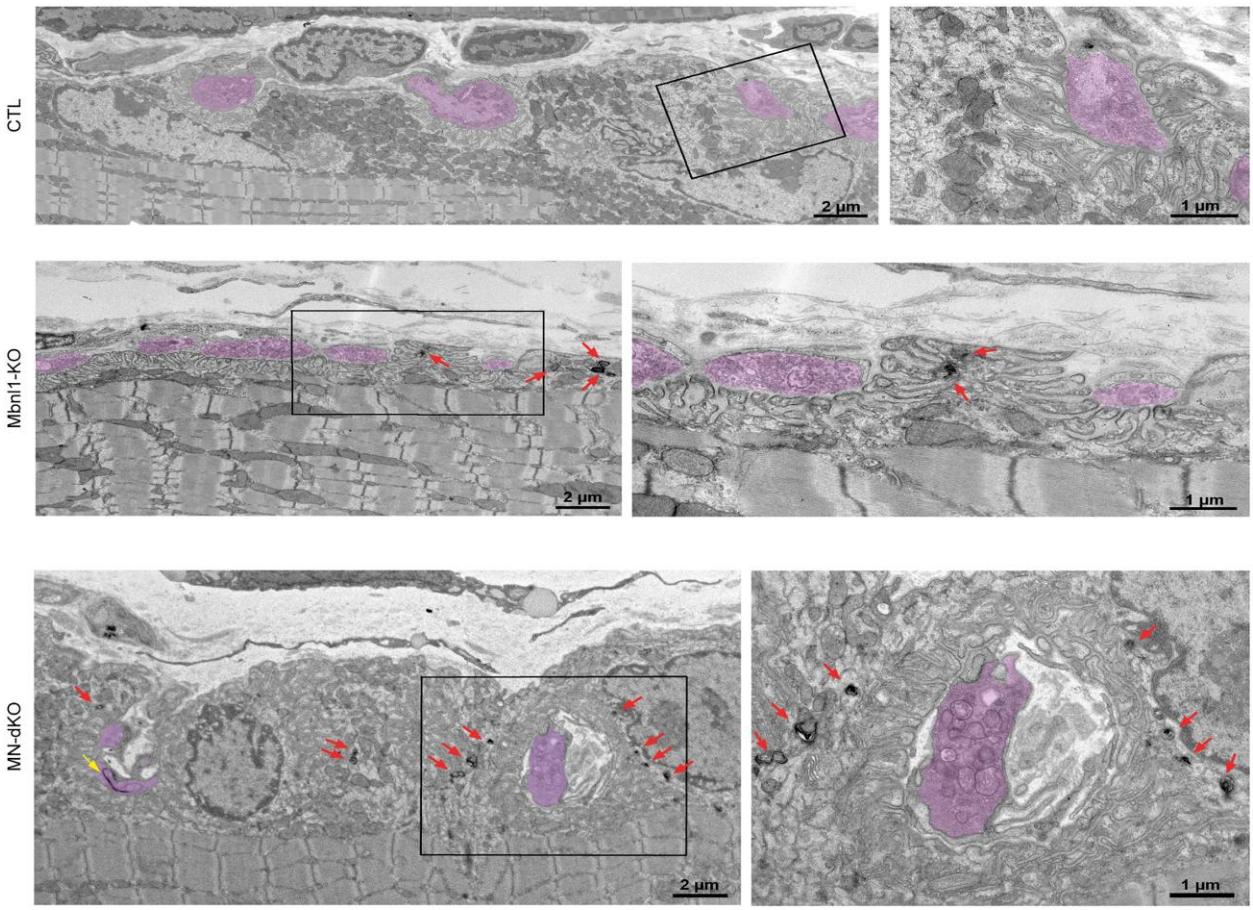

Figure 7 Additional loss of MBNL2 in motor neurons leads to neuromuscular junction ultrastructural modifications with presynaptic defects. Representative electron micrograph of neuromuscular junctions from 4-month-old control (CTL), *Mbnl1*-KO and MN-dKO tibialis anterior. Synaptic boutons are coloured purple; black squares focus on a synapse magnified on the *right*. Degenerative structures are shown by arrows in the presynaptic (yellow) and postsynaptic (red) compartments. dKO = double knockout; MN = motor neuron.

MBNL neuronal regulating pathways could be transposed from brain neurons to spinal MNs. To achieve depletion of *Mbnl2* in MNs, Hb9-Cre mice were used, given their ability to drive Cre recombinase expression predominantly in MNs as previously described.[40–46] Although it is noteworthy that a recent study shows that *Hb9* expression is not entirely exclusive to MNs and can also be expressed in other cell types in mouse spinal cord, thus RNA-sequencing data cannot be attributed solely to MNs.[52] We also report new transcripts differentially spliced following the loss of MBNL proteins and identified *Dvl1* 39 bp ex14b mis-splicing in spinal cords from MN-dKO mice. *Dvl1* codes for dishevelled segment polarity protein 1, a multi-module cytoplasmic protein crucial for Wnt canonical and non-canonical signalling.[53,54] Given that Wnt signalling is essential for NMJ maintenance,[37,55] *Dvl1* splicing alteration could participate to MN-dKO NMJ progressive defects. The molecular and physiological consequences of *Dvl1* ex14b aberrant inclusion in spinal cord remain to be determined. However, given that its inclusion produces a premature stop codon, it is likely to lead to transcript degradation through nonsense-mediated mRNA decay and a decreased expression of the DVL1 protein, as previously reported for CLCN1 mis-splicing in DM1 pathology, which causes myotonia.[11]

Although MBNL proteins regulate many alternative splicing events in MNs, we showed that combined loss of MBNL1 and MBNL2 does not impact MN cell survival *in vivo* or muscle innervation as suggested by *in vitro* models.[29] We demonstrated that MBNL proteins are required for NMJ maintenance rather than development. However, the appearance of moderate NMJ fragmentation at 2 months of age in MN-dKO mice might indicate premature impairment during early maintenance. Additionally, NMJs from *Mbnl1*-KO and MN-dKO mice showed progressive and severe AChR cluster fragmentation in 4-month-old mice. The origins of this NMJ dismantlement remains unclear, because MBNL1 is depleted from MNs and muscle in *Mbnl1*-KO and MN-dKO mice. NMJ fragmentation has been associated with massive skeletal muscle degeneration/regeneration turnover, as observed in dystrophin-deficient *mdx* mice.[56–58] However, despite the presence of a subset of muscle fibres with central nuclei, *Mbnl1*-KO mice do not exhibit overt muscle regeneration.[7,47] *MBNL1* is highly expressed in muscle tissues and co-localizes with CUGexp-RNA foci in the nuclei of DM1 muscle cells, including subsynaptic myonuclei.[26] Of interest, alternative splicing changes of transcripts coding for postsynaptic NMJ proteins, such as CHRNG and MUSK, have been reported in cell cultures from human embryonic muscle tissues carrying large CTG repeats,[59] indicating the possible contribution of CUGexp-RNA and/or MBNL1 loss in skeletal muscle to NMJ homeostasis defects. Observations of ultrastructural abnormalities in the postsynaptic compartment of 4-month-old *Mbnl1*-KO and MN-dKO mice further support the MBNL1 muscle

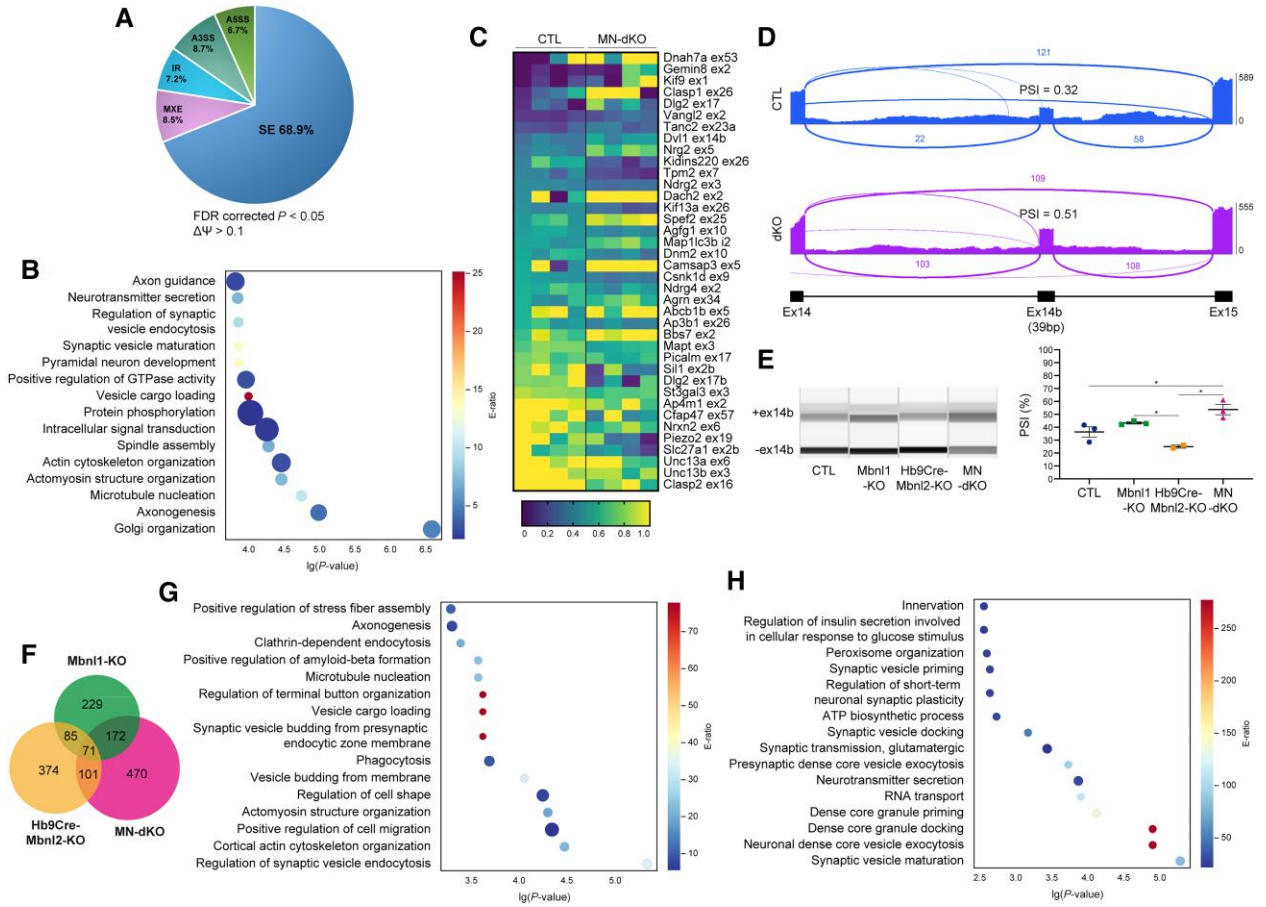

Figure 8 Alternative splicing changes in spinal cord from 4-month-old MN-dKO mice. (**A**) Pie chart represents the proportion of significant differential alternative splicing (DSE) ($\Delta\Psi > 10\%$, false discovery rate < 0.05) in 4-month-old MN-dKO mice compared with control (CTL) mice and categorized as skipped exons (SE), alternative 5′ and 3′ splice sites (A5SS and A3SS), mutually exclusive exons (MXE) and retained introns (RI). (**B**) Unbiased gene ontology (GO) top 15 biological processes involved by the differential alternative splicing events (DSE) identified in MN-dKO mice when compared with CTL mice with their corresponding *P*-values and enrichment ratio. (**C**) Heatmap shows selected DSE changed in MN-dKO mice compared with CTL mice. (**D**) Sashimi plot for Dvl1 ex14b in CTL and MN-dKO mice. (**E**) Representative RT-PCR splicing analysis of Dvl1 ex14b from CTL ($n = 3$), *Mbnl1*-KO ($n = 3$), Hb9Cre-*Mbnl2*-KO ($n = 2$) and MN-dKO mice ($n = 3$) with per cent spliced in (PSI) quantification. (**F**) Venn diagram of the number of unique genes affected in Hb9Cre-*Mbnl2*-KO, *Mbnl1*-KO and MN-dKO mice when compared with CTL mice. (**G** and **H**) The top 15 unbiased GO biological processes of genes common between MN-dKO and *Mbnl1*-KO mice (**G**) or Hb9Cre-*Mbnl2*-KO (**H**) mice are shown with their corresponding *P*-values and enrichment ratio. dKO = double knockout; MN = motor neuron.

contribution to NMJ defects. Interestingly, the HSA^{LR} mouse model, which expresses the human skeletal actin gene with expanded CTG repeats, widely used to study DM1, exhibits alterations in NMJ morphology. These alterations include destabilization of NMJs, evidenced by changes in AChR turnover and synaptic structure.[60] This suggests a retrograde effect from muscle to NMJs, which might result from MBNL sequestration by CUGexp foci within myonuclei. However, the presence of specific presynaptic abnormalities, such as nerve terminal sprouts and degenerative structures in the synaptic bouton, only in NMJs of MN-dKO mice indicates that additional loss of MBNL2 in MNs impacts the presynaptic compartment and shows the importance of MBNL dosage in MNs to NMJ maintenance. This hypothesis is strengthened by *mbl-1* (MBNL orthologue)-deficient *Caenorhabditis elegans* that exhibit NMJ defects rescued by *mbl-1* transgene when expressed specifically in presynaptic neurons and no rescue when it is expressed in muscles.[61] Lastly, although NMJ fragmentation and terminal nerve sprouting could be interpreted as NMJ degeneration markers in the rodent, it has been proposed to represent an outcome of an active repair process helping to maintain the efficiency of neuromuscular transmission.[62]

Titration of MBNL proteins by CUGexp-RNA plays a pivotal role in DM1 pathogenesis, and most of the DM1 splicing abnormalities are attributable to MBNL loss of function.[63] Nuclear CUGexp-RNA foci that co-localize with MBNL1 have been found in DM1 MNs[26] and electron microscopy analysis showed modifications of motor end-plate size and NMJ , in addition to neurotransmission defects in affected muscles of DM1 patients.[21–24,64] Loss of MBNL proteins, and notably loss of MBNL2, in mice have recapitulated DM1 neurological features associated with similar splicing abnormalities.[16,17] Moreover, loss of MBNL1 and MBNL2 in MNs alters alternative splicing of genes involved in synaptic vesicle maturation and endocytosis, key biological processes involved in neurodegeneration in DMSXL mice and DM1 patients.[65,66] Of interest, several mis-splicing events found in spinal cords of MN-dKO mice, such as MAPT, SORBS1 and TANC2, have been previously reported in brains from DM1 patients[51,67–70] and DMSXL mice.[36,65] Alternative splicing abnormalities associated with DM1 CNS impairments suggest that RNA modifications described in the DM1 brain might also occur in DM1 spinal cord and contribute to pathogenesis. Interestingly, alternative splicing modifications of MAPT, SORBS1 and WNK1, among others, have also been reported in motor neurons isolated

from the spinal cords of DM1 patients. Additionally, increased expression of genes related to immunity, such as *ENDOU*, *MKI67*, *CD300LF* and *LCN2*, are observed in DM1 motor neurons and in the spinal cords of MN-dKO mice.[27] In addition, MN-dKO mice develop early gait coordination abnormalities that worsen over time, with alterations of the choice of paws used for and distance between footfalls (e.g. walking pattern and stride length), in addition to increased hind stand duration that could be accompanied by the increase of front/hind paw distance. These observations are reminiscent of the typical 'dragging of the hind body' seen in spinal cord injury models.[71–74] Furthermore, disturbances of gait and balance are an important component of DM1 disease[75–79] that have recently been associated with a deterioration of the CNS–skeletal muscle network. This might reflect reduced CNS ability to segregate signals to distinct motor control modules without correlation with muscle weakness.[80] In this study, we not only showed that MBNL loss leads to progressive gait deficiencies but also that aggravated balance defects and muscle weakness arise primarily from the combined loss of both MBNL1 and MBNL2 in MNs, suggesting that MBNL sequestration in DM1 MNs might contribute to the motor and mobility difficulties of DM1 patients.

Conclusion

In conclusion, our results demonstrate the importance of MBNL dosage in motor unit homeostasis. This work provides new insights into MN involvement in DM1 disease and into potential therapeutic targets and strategies for DM treatment, with the ultimate goal of preserving motor function and improving patient outcomes.

Data availability

The data that support the findings of this study are available from the corresponding author, upon reasonable request.

Acknowledgements

Imaging was performed at the Service Commun de Microscopie (SCM) imaging platform of Université Paris Cité. We thank I. Holt and G. Morris (The Wolfson Center for Inherited Neuromuscular Disease, Robert Jones and Agnes Hunt Orthopaedic Hospital, UK) as well as 'The Muscular Dystrophy Association Monoclonal Antibody Resource' for the MBNL2 antibody, C. Thornton for the MBNL1 polyclonal antibody, the iGenSeq facility and Data analysis core of the Institut du Cerveau (Paris, France), Repeat expansions and myotonic dystrophy team, C. Legay and S. Godard-Bauché for fruitful discussions.

Funding

This work was supported by grants from ANR (Agence Nationale de la Recherche, 'motor-DM' project ANR-20-CE12-0002 to F.R.), AFM-Téléthon (Association Francaise contre les Myopathies) and Association Institut de Myologie. C.F.R. was supported by the Fondation pour la Recherche Médicale (FRM).

Competing interests

The authors declare no conflicts of interest.

Supplementary material

Supplementary material is available at *Brain* online.

References

1. Fardaei M, Rogers MT, Thorpe HM, Larkin K, Hamshere MG, Harper PS, Brook JD Three proteins, MBNL, MBLL and MBXL, co-localize *in vivo* with nuclear foci of expanded-repeat transcripts in DM1 and DM2 cells. *Hum Mol Genet*. 2002;11:805-814.
2. Batra R, Charizanis K, Manchanda M, et al. Loss of MBNL leads to disruption of developmentally regulated alternative polyadenylation in RNA-mediated disease. *Mol Cell*. 2014;56:311-322.
3. Klein AF, Gasnier E, Furling D. Gain of RNA function in pathological cases: Focus on myotonic dystrophy. *Biochimie*. 2011;93:2006-2012.
4. Rau F, Freyermuth F, Fugier C, et al. Misregulation of miR-1 processing is associated with heart defects in myotonic dystrophy. *Nat Struct Mol Biol*. 2011;18:840-845.
5. Wang ET, Cody NAL, Jog S, et al. Transcriptome-wide regulation of pre-mRNA splicing and mRNA localization by muscleblind proteins. *Cell*. 2012;150:710-724.
6. Konieczny P, Stepniak-Konieczna E, Sobczak K. MBNL proteins and their target RNAs, interaction and splicing regulation. *Nucleic Acids Res*. 2014;42:10873-10887.
7. Lee KY, Li M, Manchanda M, et al. Compound loss of muscleblind-like function in myotonic dystrophy. *EMBO Mol Med*. 2013;5:1887-1900.
8. Thomas JD, Sznajder ŁJ, Bardhi O, et al. Disrupted prenatal RNA processing and myogenesis in congenital myotonic dystrophy. *Genes Dev*. 2017;31:1122-1133.
9. Harper PS. *Myotonic Dystrophy*. 3rd ed. OUP; 2001.
10. Brook JD, McCurrach ME, Harley HG, et al. Molecular basis of myotonic dystrophy: Expansion of a trinucleotide (CTG) repeat at the 3′ end of a transcript encoding a protein kinase family member. *Cell*. 1992;68:799-808.
11. Charlet-B N, Savkur RS, Singh G, Philips AV, Grice EA. Loss of the muscle-specific chloride channel in type 1 myotonic dystrophy due to misregulated alternative splicing. *Mol Cell*. 2002;10:45-53.
12. Freyermuth F, Rau F, Kokunai Y, et al. Splicing misregulation of *SCN5A* contributes to cardiac-conduction delay and heart arrhythmia in myotonic dystrophy. *Nat Commun*. 2016;7:11067.
13. Fugier C, Klein AF, Hammer C, et al. Misregulated alternative splicing of *BIN1* is associated with T tubule alterations and muscle weakness in myotonic dystrophy. *Nat Med*. 2011;17:720-725.
14. Rau F, Lainé J, Ramanoudjame L, et al. Abnormal splicing switch of DMD's penultimate exon compromises muscle fibre maintenance in myotonic dystrophy. *Nat Commun*. 2015;6:7205.
15. Tang ZZ, Yarotskyy V, Wei L, et al. Muscle weakness in myotonic dystrophy associated with misregulated splicing and altered gating of $Ca_V1.1$ calcium channel. *Hum Mol Genet*. 2012;21:1312-1324.
16. Charizanis K, Lee K-Y, Batra R, et al. Muscleblind-like 2-mediated alternative splicing in the developing brain and dysregulation in myotonic dystrophy. *Neuron*. 2012;75:437-450.
17. Goodwin M, Mohan A, Batra R, et al. MBNL sequestration by toxic RNAs and RNA misprocessing in the myotonic dystrophy brain. *Cell Rep*. 2015;12:1159-1168.
18. Sta Maria NS, Zhou C, Lee SJ, et al. Mbnl1 and Mbnl2 regulate brain structural integrity in mice. *Commun Biol*. 2021;4:1342.
19. Lee K-Y, Seah C, Li C, et al. Mice lacking MBNL1 and MBNL2 exhibit sudden cardiac death and molecular signatures recapitulating myotonic dystrophy. *Hum Mol Genet*. 2022;31:3144-3160.

20. Lee KY, Chang HC, Seah C, Lee LJ. Deprivation of muscleblind-like proteins causes deficits in cortical neuron distribution and morphological changes in dendritic spines and postsynaptic densities. *Front Neuroanat*. 2019;13:75.
21. Allen DE, Johnson AG, Woolf AL. The intramuscular nerve endings in dystrophia myotonica—a biopsy study by vital staining and electron microscopy. *J Anat*. 1969;105:1-26.
22. Fardeau M, Tomé F. Light and electron microscopic study of motor endplates in the adult and neonatal forms of dystrophia myotonica, In: *Ontogenesis and functional mechanisms of peripheral synapses*. Elsevier/North-Holland Biomedical Press; 1980:287-298.
23. Macdermot V. The histology of the neuromuscular junction in dystrophia myotonica. *Brain*. 1961;84:75-84.
24. Bombelli F, Lispi L, Porrini SC, et al. Neuromuscular transmission abnormalities in myotonic dystrophy type 1: A neurophysiological study. *Clin Neurol Neurosurg*. 2016;150:84-88.
25. Krishnan AV, Kiernan MC. Axonal function and activity-dependent excitability changes in myotonic dystrophy. *Muscle Nerve*. 2006;33:627-636.
26. Wheeler TM, Krym MC, Thornton CA. Ribonuclear foci at the neuromuscular junction in myotonic dystrophy type 1. *Neuromuscul Disord*. 2007;17:242-247.
27. Nakamori M, Shimizu H, Ogawa K, et al. Cell type-specific abnormalities of central nervous system in myotonic dystrophy type 1. *Brain Commun*. 2022;4:1-17.
28. Panaite PA, Gantelet E, Kraftsik R, Gourdon G, Kuntzer T, Barakat-Walter I. Myotonic dystrophy transgenic mice exhibit pathologic abnormalities in diaphragm neuromuscular junctions and phrenic nerves. *J Neuropathol Exp Neurol*. 2008;67:763-772.
29. Tahraoui-Bories J, Mérien A, González-Barriga A, et al. MBNL-dependent impaired development within the neuromuscular system in Myotonic Dystrophy type 1. *Neuropathol Appl Neurobiol*. 2022;49:e12876.
30. Delacroix C, Hyzewicz J, Lemaitre M, et al. Improvement of dystrophic muscle fragility by short-term voluntary exercise through activation of calcineurin pathway in *mdx* mice. *Am J Pathol*. 2018;188:2662-2673.
31. Xie Z, Bailey A, Kuleshov MV, et al. Gene set knowledge discovery with Enrichr. *Curr Protoc*. 2021;1:e90.
32. Chen EY, Tan CM, Kou Y, et al. Enrichr: Interactive and collaborative HTML5 gene list enrichment analysis tool. *BMC Bioinformatics*. 2013;14:128.
33. Ashburner M, Ball CA, Blake JA, et al. Gene ontology: Tool for the unification of biology. The Gene Ontology Consortium. *Nat Genet*. 2000;25:25-29.
34. Gene Ontology Consortium. The gene ontology resource: Enriching a GOld mine. *Nucleic Acids Res*. 2021;49:D325-D334.
35. Ning W, Wei Y, Gao L, et al. Hemi 2.0: An online service for heatmap illustration. *Nucleic Acids Res*. 2022;50:W405-W411.
36. Dinca DM, Lallemant L, González-Barriga A, et al. Myotonic dystrophy RNA toxicity alters morphology, adhesion and migration of mouse and human astrocytes. *Nat Commun*. 2022;13:3841.
37. Messéant J, Dobbertin A, Girard E, et al. Musk frizzled-like domain is critical for mammalian neuromuscular junction formation and maintenance. *J Neurosci*. 2015;35:4926-4941.
38. Boëx M, Cottin S, Halliez M, et al. The cell polarity protein Vangl2 in the muscle shapes the neuromuscular synapse by binding to and regulating the tyrosine kinase MuSK. *Sci Signal*. 2022;15:eabg4982.
39. Besse A, Astord S, Marais T, et al. AAV9-mediated expression of SMN restricted to neurons does not rescue the spinal muscular atrophy phenotype in mice. *Molecular Therapy*. 2020;28:1887-1901.
40. Bolis A, Coviello S, Bussini S, et al. Loss of Mtmr2 phosphatase in Schwann cells but not in motor neurons causes Charcot-Marie-Tooth type 4B1 neuropathy with myelin outfoldings. *J Neurosci*. 2005;25:8567-8577.
41. Cheever TR, Olson EA, Ervasti JM. Axonal regeneration and neuronal function are preserved in motor neurons lacking ß-actin *in vivo*. *PLoS One*. 2011;6:e17768.
42. Chipman PH, Franz CK, Nelson A, Schachner M, Rafuse VF. Neural cell adhesion molecule is required for stability of reinnervated neuromuscular junctions. *Eur J Neurosci*. 2010;31:238-249.
43. Hess DM, Scott MO, Potluri S, Pitts EV, Cisterni C, Balice-Gordon RJ. Localization of TrkC to Schwann cells and effects of neurotrophin-3 signaling at neuromuscular synapses. *J Comp Neurol*. 2007;501:465-482.
44. Luria V, Laufer E. Lateral motor column axons execute a ternary trajectory choice between limb and body tissues. *Neural Dev*. 2007;2:13.
45. Mende Y, Jakubik M, Riessland M, et al. Deficiency of the splicing factor Sfrs10 results in early embryonic lethality in mice and has no impact on full-length SMN/Smn splicing. *Hum Mol Genet*. 2010;19:2154-2167.
46. Li XM, Dong X-P, Luo S-W, et al. Retrograde regulation of motoneuron differentiation by muscle β-catenin. *Nat Neurosci*. 2008;11:262-268.
47. Kanadia RN, Johnstone KA, Mankodi A, et al. A muscleblind knockout model for myotonic dystrophy. *Science*. 2003;302:1978-1980.
48. Choi J, Personius KE, DiFranco M, et al. Muscleblind-like 1 and muscleblind-like 3 depletion synergistically enhances myotonia by altering *Clc-1* RNA translation. *EBioMedicine*. 2015;2:1034-1047.
49. Denes LT, Kelley CP, Wang ET. Microtubule-based transport is essential to distribute RNA and nascent protein in skeletal muscle. *Nat Commun*. 2021;12:6079.
50. Taliaferro J. M., Vidaki M., Oliveira R., et al. Distal alternative last exons localize mRNAs to neural projections. *Molec Cell*. 2016;61(6):821–833.
51. Suenaga K, Lee K-Y, Nakamori M, et al. Muscleblind-like 1 knockout mice reveal novel splicing defects in the myotonic dystrophy brain. *PLoS One*. 2012;7:e33218.
52. Letchuman S, Tucker A, Miranda D, et al. Transcription factor Hb9 is expressed in glial cell lineages in the developing mouse spinal cord. *eNeuro*. 2022;9:ENEURO.0214-22.2022.
53. Shafer B, Onishi K, Lo C, Colakoglu G, Zou Y. Vangl2 promotes Wnt/planar cell polarity-like signaling by antagonizing dvl1-mediated feedback inhibition in growth cone guidance. *Dev Cell*. 2011;20:177-191.
54. Wang W, Li X, Lee M, et al. FOXKs promote Wnt/β-catenin signaling by translocating DVL into the nucleus. *Dev Cell*. 2015;32:707-718.
55. Shen C, Li L, Zhao K, et al. Motoneuron Wnts regulate neuromuscular junction development. *Elife*. 2018;7:e34625.
56. Pratt SJP, Shah SB, Ward CW, Inacio MP, Stains JP, Lovering RM. Effects of *in vivo* injury on the neuromuscular junction in healthy and dystrophic muscles. *J Physiol*. 2013;591:559-570.
57. Pratt SJP, Valencia AP, Le GK, Shah SB, Lovering RM. Pre- and postsynaptic changes in the neuromuscular junction in dystrophic mice. *Front Physiol*. 2015;6:252.
58. Pratt SJP, Shah SB, Ward CW, Kerr JP, Stains JP, Lovering RM. Recovery of altered neuromuscular junction morphology and muscle function in *mdx* mice after injury. *Cell Mol Life Sci*. 2014;72:153-164.

59. Klinck R, Fourrier A, Thibault P, et al. RBFOX1 cooperates with MBNL1 to control splicing in muscle, including events altered in myotonic dystrophy type 1. *PLoS One*. 2014;9:18-21.
60. Falcetta D, Quirim S, Cocchiararo I, et al. CaMKIIβ deregulation contributes to neuromuscular junction destabilization in Myotonic Dystrophy type I. *Skelet Muscle*. 2024;14:11.
61. Spilker KA, Wang GJ, Tugizova MS, Shen K. *Caenorhabditis elegans* Muscleblind homolog *mbl-1* functions in neurons to regulate synapse formation. *Neural Dev*. 2012;7:7.
62. Slater CR. 'Fragmentation' of NMJs: A sign of degeneration or regeneration? A long journey with many junctions. *Neuroscience*. 2020;439:28-40.
63. Nakamori M, Sobczak K, Puwanant A, et al. Splicing biomarkers of disease severity in myotonic dystrophy. *Ann Neurol*. 2013;74:862-872.
64. Kanning KC, Kaplan A, Henderson CE. Motor neuron diversity in development and disease. *Annu Rev Neurosci*. 2010;33:409-440.
65. Hernández-Hernández O, Guiraud-Dogan C, Sicot G, et al. Myotonic dystrophy CTG expansion affects synaptic vesicle proteins, neurotransmission and mouse behaviour. *Brain*. 2013;136:957-970.
66. Jimenez-Marin A, Diez I, Labayru G, et al. Transcriptional signatures of synaptic vesicle genes define myotonic dystrophy type I neurodegeneration. *Neuropathol Appl Neurobiol*. 2021;47:1092-1108.
67. Caillet-Boudin M-L, Fernandez-Gomez F-J, Tran H, Dhaenens C-M, Buee L, Sergeant N. Brain pathology in myotonic dystrophy: When tauopathy meets spliceopathy and RNAopathy. *Front Mol Neurosci*. 2014;6:57.
68. Dhaenens CM, Tran H, Frandemiche M-L, et al. Mis-splicing of Tau exon 10 in myotonic dystrophy type 1 is reproduced by overexpression of CELF2 but not by MBNL1 silencing. *Biochim Biophys Acta*. 2011;1812:732-742.
69. Jiang H, Mankodi A, Swanson MS, Moxley RT, Thornton CA. Myotonic dystrophy type 1 is associated with nuclear foci of mutant RNA, sequestration of muscleblind proteins and deregulated alternative splicing in neurons. *Hum Mol Genet*. 2004;13:3079-3088.
70. Sergeant N, Sablonnière B, Schraen-Maschke S, et al. Dysregulation of human brain microtubule-associated tau mRNA maturation in myotonic dystrophy type 1. *Hum Mol Genet*. 2001;10:2143-2155.
71. Kloos AD, Fisher LC, Detloff MR, Hassenzahl DL, Basso DM. Stepwise motor and all-or-none sensory recovery is associated with nonlinear sparing after incremental spinal cord injury in rats. *Exp Neurol*. 2005;191:251-265.
72. Lee H, McKeon RJ, Bellamkonda RV. Sustained delivery of thermostabilized chABC enhances axonal sprouting and functional recovery after spinal cord injury. *Proc Natl Acad Sci U S A*. 2010;107:3340-3345.
73. Hamers FP, Lankhorst AJ, van Laar TJ, Veldhuis WB, Gispen WH. Automated quantitative gait analysis during overground locomotion in the rat: Its application to spinal cord contusion and transection injuries. *J Neurotrauma*. 2001;18:187-201.
74. Hamers FPT, Koopmans GC, Joosten EAJ. CatWalk-assisted gait analysis in the assessment of spinal cord injury. *J Neurotrauma*. 2006;23:537-548.
75. Wright RB, Yoder DM, Costa JL, Andriacchi TP. Characterization of gait parameters in adult-onset myotonic dystrophy: Abnormal hip motion. *Arch Phys Med Rehabil*. 1995;76:33-38.
76. Galli M, Cimolin V, Crugnola V, et al. Gait pattern in myotonic dystrophy (Steinert disease): A kinematic, kinetic and EMG evaluation using 3D gait analysis. *J Neurol Sci*. 2012;314:83-87.
77. Bachasson D, Moraux A, Ollivier G, et al. Relationship between muscle impairments, postural stability, and gait parameters assessed with lower-trunk accelerometry in myotonic dystrophy type 1. *Neuromuscul Disord*. 2016;26:428-435.
78. Pucillo EM, Mcintyre MM, Pautler M, et al. Modified dynamic gait index and limits of stability in myotonic dystrophy type 1. *Muscle and Nerve*. 2018;58:694-699.
79. Bassez G, Audureau E, Hogrel J-Y, et al. Improved mobility with metformin in patients with myotonic dystrophy type 1: A randomized controlled trial. *Brain*. 2018;141:2855-2865.
80. Naro A, Portaro S, Milardi D, et al. Paving the way for a better understanding of the pathophysiology of gait impairment in myotonic dystrophy: A pilot study focusing on muscle networks. *J Neuroeng Rehabil*. 2019;16:116.